Received: 21 November 2025 | Revised: 7 January 2026 | Accepted: 26 January 2026 | Published online: 18 March 2026

RESEARCH ARTICLE

Smart Wearable Technology
2026, Vol. 00(00) 1–16
DOI: 10.47852/bonviewSWT62028348

BON VIEW PUBLISHING

Verification of the Self-Load Assessment Capability of Inertial Measurement Units via Lumbar Musculoskeletal Simulation

Zhong Wang[1], Xiaohuan Yuan[2,*], Yuanliang Tang[1,3,*] and Shaohui Zhang[1,4,*]

[1] *The Institute of Biological and Medical Engineering, Guangdong Academy of Sciences, China*

[2] *College of Life Sciences, Mudanjiang Medical University, China*

[3] *Tai'an Nuotai Electronic Technology Co., Ltd., China*

[4] *Key Laboratory of Nanodevices and Applications, Suzhou Institute of Nano-Tech and Nano-Bionics, China*

Abstract: This study aims to validate the capability of inertial measurement units (IMUs) combined with surface electromyography (sEMG) sensors for assessing lumbar self-load. Lumbar biomechanical simulation was performed using OpenSim software, and data collected by IMUs and sEMG sensors were integrated into the simulation to evaluate the system's performance in assessing lumbar load under static postures in real environments. In the experiment, 15 IMUs were fixed at human anatomical landmarks, and motion data and sEMG signals were synchronously collected during isometric tests of lumbar muscles. IMU data were converted into an OpenSim-compatible format through a self-developed processing workflow to realize musculoskeletal dynamic and kinematic analysis. The experiment included four types of static posture tests, and six sets of isometric test motion data were collected. The results showed that under different static postures, the L1–L5 lumbar joints remained stable, the distribution of joint driving torque showed a regular pattern, and the muscle driving forces were different and basically consistent with physiological reality; sEMG signal analysis verified the evaluation capability of the system, and the muscle fatigue characteristics were consistent with expectations. This study confirms the methodological effectiveness of the combination of IMU and sEMG sensors for static lumbar load assessment in real environments, providing a potential methodological reference for the clinical evaluation of nonspecific low back pain.

Keywords: bio-information processing, biomechanics, inertial measurement units (IMUs), musculoskeletal modeling and simulation, surface electromyography (sEMG) sensors

1. Introduction

Biomechanical simulation is a technology based on biomechanical principles that uses mathematical models and computer simulation techniques to reproduce a series of mechanical behaviors of biological systems, including the stress state of biological structural materials, movement laws, and neuromuscular control. This technology is widely used in fields such as medicine, biology, neuroscience, sports rehabilitation, mechanics, and robotics [1].

OpenSim is an open-source software platform specifically designed for biomechanical modeling and simulation, developed and maintained by the National Center for Biomedical Computing (Simbios) at Stanford University. It aims to help researchers and clinicians better understand and analyze human movement and its underlying physiological mechanisms. OpenSim has advantages in biomechanical modeling, motion simulation, biomechanical analysis, and optimal control. Its built-in inverse solution method applies experimentally measured motion data to the musculoskeletal model system for biomechanical calculations, thereby providing ideal evaluation results for the musculoskeletal system [2].

However, traditional motion capture (MoCap) systems usually rely on equipment based on optical markers and optical sensors. Although the optical motion capture (OMC) system is regarded as the gold standard for motion capture, it has many limitations: the equipment is expensive and unaffordable for small studios or individuals; it requires special deployment in a specific, unobstructed environment; and it is only applicable to fixed laboratory scenarios and cannot meet the real-time monitoring needs in real working environments [3, 4]. In contrast, inertial measurement units (IMUs) as miniaturized wearable sensors have

*Corresponding authors: Xiaohuan Yuan, College of Life Sciences, Mudanjiang Medical University, China. Email: yuanxiaohuan@mdjmu.edu.cn, Yuanliang Tang, The Institute of Biological and Medical Engineering, Guangdong Academy of Sciences and Tai'an Nuotai Electronic Technology Co., Ltd., China. Email: nuotaikeji@nuotai.biz and Shaohui Zhang, The Institute of Biological and Medical Engineering, Guangdong Academy of Sciences and Key Laboratory of Nanodevices and Applications, Suzhou Institute of Nano-Tech and Nano-Bionics, China. Email: shzhang2016@sinano.ac.cn

the advantages of small size, light weight, and no restriction by specific environments (such as no need for special camera equipment). They can replace OMC equipment to realize biological information collection in real working environments. An IMU usually includes a gyroscope and an accelerometer, and adding a magnetometer can further determine the geographical orientation and reduce the cumulative error of acceleration and angular velocity [5, 6].

In recent years, portable IMU sensors have attracted widespread attention in biomechanical research due to their great potential [7–10]. In the biomedical field, surface electromyography (sEMG) is an indicator for evaluating neuromuscular activation characteristics during skeletal muscle activity, and the intensity of sEMG signals usually reflects the degree of muscle activation. sEMG sensors are commonly used measurement tools in ergonomics and related fields. By analyzing sEMG information during fatigue, the neuromuscular function state and activity level can be evaluated, which is an effective noninvasive method for quantitatively assessing the relationship between external muscle load and internal response [11–14].

In recent years, with the rapid development of wearable technology, the application of IMU and sEMG sensors in lumbar load assessment has received increasing attention. For example, Shariatzadeh et al. [15]. designed a wearable system integrating sEMG and motion sensors, using the wavelet analysis method. In the bicep curl experiment of healthy adults, they found that the normalized energy of sEMG signals obtained by wavelet decomposition can quantitatively predict muscle fatigue during dynamic contraction, providing an effective means for fatigue assessment in this scenario. Zhang et al. [16] used the OpenSim model combined with the OMC system to evaluate lumbar load during walking in patients with chronic low back pain and healthy controls and found that the distribution of lumbar joint forces was different from that in static postures. In addition, Urukalo et al. [17] carried out a study on human activity estimation based on a single sensor for workers' low back pain risk assessment: a wearable IMU sensor was worn on the back, the sensor position was optimized using avatar data, and a 2D CNN-BiLSTM model was applied to identify activities in warehouse two-arm operation experiments. Without sEMG, the recognition accuracy for 54 low-variability activity categories reached 91.77%, providing a solution for cost-effective wearable devices. Fujii et al. [18] proposed a lumbar power-assisted exoskeleton control method, using a 9-axis IMU sensor (replacing sEMG) combined with Convolutional Neural Network (CNN) and Long Short-Term Memory (LSTM) models for posture classification. In the lifting test of 10 subjects, it significantly reduced the integrated electromyographic activity and realized lumbar motion assistance. These studies show that IMU and sEMG sensors have broad application prospects in lumbar load assessment, but existing studies mostly focus on specific dynamic tasks or the application of special equipment, and there is still a gap in the assessment of static lumbar load in real working environments. This study aims to fill this gap by combining IMU and sEMG sensors and using OpenSim for musculoskeletal simulation to verify their ability to assess lumbar self-load under static postures in real environments, providing new methods and perspectives for the clinical evaluation of nonspecific low back pain.

The human lumbar musculoskeletal system undertakes the important functions of supporting the upper body and head and realizing flexion, bending, and rotation [19, 20]. However, changes in modern living and office environments and the extension of human life expectancy have led to more people being in static postures for a long time (such as office work), which has significantly increased the incidence of chronic nonspecific low back pain [21, 22]. The proportion of low back pain in occupational diseases is increasing day by day, and prolonged sitting and poor working postures are considered the main pathogenic factors [23–26]. In modern industrialized countries, the prevalence of low back pain is about 40%, of which nonspecific low back pain accounts for more than 70% [27, 28]. Although a large number of studies have focused on the load of the lumbar spine and muscles, most existing assessment methods cannot meet the needs in real working environments. For example, the OMC system cannot be applied to real-time monitoring in real office environments, and special force measurement equipment is not suitable for normal office scenarios [29]. Therefore, miniaturized wearable IMU sensors are ideal devices for collecting biological information in real working environments, and their portability can minimize interference with work tasks.

In practical applications, direct, accurate, and detailed mechanical measurement of skeletal joints or muscles is impractical. Therefore, it is necessary to conduct a noninvasive assessment of the lumbar musculoskeletal system based on models integrating human anatomy, biomechanics, kinematics, and mechanical principles. This study uses a detailed lumbar musculoskeletal model supported by OpenSim software as the simulation carrier, takes IMU and sEMG sensors as input sources, and imports data into a personalized OpenSim musculoskeletal model to verify the lumbar self-load assessment capability based on IMU and sEMG sensors. By analyzing the experimentally collected data, the lumbar joint angle, torque, and muscle driving force under different static postures are evaluated to provide assistance and guidance for the clinical evaluation of nonspecific low back pain.

2. Materials and Methods

2.1. Subjects

Four healthy male volunteers participated in the experiment (aged 25 ± 1 years; height: 174 ± 4 cm; weight: 65 ± 5 kg). All subjects had no history of low back pain, trauma, or pain, did not engage in strenuous physical activity one week before the experiment, and signed informed consent forms.

2.2. Instruments and materials

An IMU system (REBOCAP, Jiangsu, China) was used to collect motion data, which included 15 sensors for capturing motion information. The preprocessing of motion capture included standardized sensor placement and calibration procedures. A dual-channel sEMG system (Sichirray, Wuxi, China) was used to record sEMG activity in the lumbar erector spinae region of the subjects.

Auxiliary materials used in the experiment included Ag/AgCl electrodes, 95% ethanol, paper towels, a stopwatch, and a motion platform to assist in recording the subjects' experimental movements. sEMG data were recorded and processed on a computer running the Windows operating system.

2.3. Loads and tasks

All tasks in the experiment were completed using the subject's own body weight. The posterior lumbar muscles mainly include the multifidus, erector spinae, and iliocostalis lumborum (IL). Static isometric tests were used [30–32] (dynamic components were excluded because this study focuses on static postures).

Static motion data and sEMG signals were collected during the execution of tasks for six body postures involving lumbar muscles

in four groups, namely: quiet standing, quiet sitting, right lateral bridge, left lateral bridge, right bird-dog, and left bird-dog [33, 34]. Before the test, the subjects were instructed on posture standards and electrode placement methods. After skin preparation with 95% ethanol, sEMG electrodes were attached to the designated positions. During the test, the subjects first lay supine on a yoga mat to relax, entered the target posture and maintained it upon instruction, and timing began. After completing each posture, the subjects rested for at least 10 min to ensure complete muscle recovery, and the entire test process was repeated twice. Before the test, the subjects were guided on maintaining standard postures, and researchers monitored the entire test process to ensure the subjects maintained correct postures.

2.4. Motion data collection

Motion data processing was realized through the process of IMU capture, Python script-based data conversion, and transmission of marker trajectories to OpenSim.

Each IMU sensor adopted a 9-degree-of-freedom unit with a magnetic field calibration function, consisting of a 3-axis accelerometer, a 3-axis gyroscope, and a 3-axis geomagnetic sensor [35]. This study was based on motion data in BVH (Biovision Hierarchy) format output by the device host software. (The placement position of IMU sensors is shown in Figure 1).

Figure 1
Photo of the experimental participant wearing IMU sensors and a dual-channel sEMG sensor

2.5. Motion data conversion

The motion data captured by the IMU system were encapsulated in BVH format. BVH is a common output data format for biomechanical motion capture equipment. The human skeletal model is described as a virtual humanoid topological structure framework defined based on 24 nodes; 15 IMUs were placed on designated body segments, respectively. BVH files store bone (structure) and motion (data) information. Each BVH file includes two parts: bone information describing the hierarchical structure of key nodes of the human skeleton (Figure 2), where nodes are defined recursively, and a data block containing information of these key nodes, recording the position and rotation information of each node per frame. Motion is described by parameters such as OFFSET (relative displacement between the node and the root node ROOT) and CHANNELS. CHANNELS usually include six items: three position coordinates and three Euler angles representing rotation [36–38].

Figure 2
Topological diagram of the BVH skeletal structure exported by IMU sensors, characterized by "key nodes"

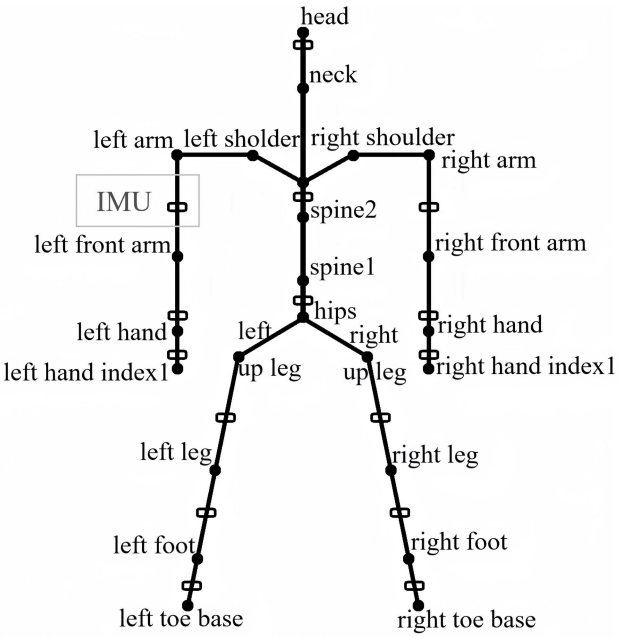

The first step of data conversion was to convert the position information in the BVH file into a comma-separated values (CSV) file under the world coordinate system for OpenSim to read. The open-source Python script "BVH-converter" was used to convert the BVH file coordinates to world position (worldpos), and then the world coordinate system CSV file containing node motion information was converted into an OpenSim marker trajectory (.trc) file. The complete processing flow is shown in Figure 3.

2.6. Lumbar joints inverse kinematics

The experimental dataset included six static self-load postures: quiet standing, quiet sitting, right lateral bridge, left lateral bridge, right bird-dog, and left bird-dog (as shown in Figure 4). Information on L1–L5 lumbar joints was extracted for feature analysis, and Figure 5 shows the angle changes of lumbar joints

Figure 3
Flowchart of converting the BVH dataset to OpenSim marker files. The original motion BVH data are processed through a two-stage Python script and finally generate .trc files compatible with OpenSim 4.5

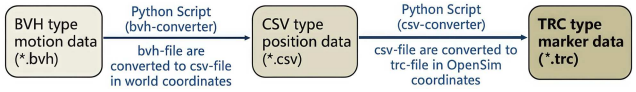

Figure 4
Schematic diagrams of experimental postures: (a) quiet standing, (b) quiet sitting, (c) bird-dog, and (d) lateral bridge

Figure 5
Temporal evolution of lumbar joint angles during three movement tests: (a) quiet standing, (b) left lateral bridge, and (c) left bird-dog

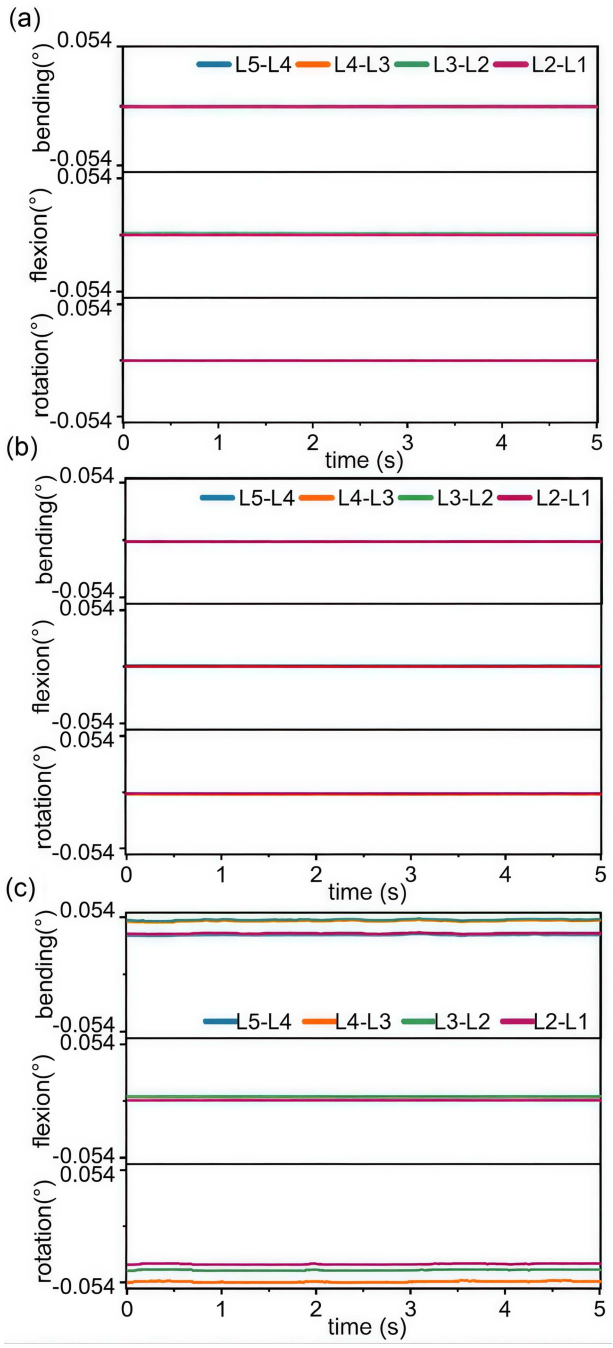

under three postures. Lumbar joint inverse kinematics data within a stable 5-second window were extracted.

The OpenSim musculoskeletal model used to evaluate the lumbar system in this study was the publicly available OpenSim "full-body lumbar musculoskeletal model," which has complete muscle tissue and lumbar degrees of freedom, with five lumbar joints modeled separately. The overall lumbar motion includes flexion, axial rotation, and bending.

2.7. Lumbar joint inverse dynamics

The initial solution method for inverse kinematics adopted the calculation method used in the OMC system. Since the experiment measured static postures, it was considered unnecessary to perform filtering processing other than standard preprocessing on the sensor data.

The motion of the OpenSim model is determined by its generalized coordinates, velocities, and accelerations. The inverse dynamics tool solves the motion equation using the known model motion (inverse kinematics output results) to obtain the unknown generalized forces [39–41].

2.8. Lumbar joints static optimization

To characterize the ability of IMU-based marker data to assess human lumbar biomechanics, this study analyzed the static

optimization results, especially the forces exerted by the muscles responsible for lumbopelvic stability in the model.

For the right and left lateral bridge postures, the driving forces of the IL pars lumborum and longissimus thoracis pars lumborum (LTpL), which are responsible for lumbar stability and support in the model, on the L1–L5 lumbar joints, as well as the forces on the intervertebral discs between L1–L5 lumbar joints when driven, were adopted, respectively.

For comparative analysis, the joint forces of L1–L4 intervertebral discs (IL) or L1–L5 intervertebral discs (LTpL) under different postures in the same group were averaged within a 1-second time domain (60 data points) to obtain the overall lumbar joint force measurement value. The effectiveness of the method was verified by comparing the overall average joint forces under the two postures.

The average value of the four joint forces was the average within 60 frames, where "f" is the number of frames in 1 second, "lbr" is the number of lumbar joints, and "$IL\_L_1\_l_1$" is the joint force of the left lumbar L1 in the first frame of data. The overall average joint force was used to normalize different postures:

$$\text{mean\_AVG}_r = \frac{1}{60}\left\{\sum_{\text{f}=1}^{60}\left[\frac{1}{4}\left(\sum_{\text{lbr}=1}^{4}\text{IL\_L}_{\text{lbr}}\text{\_r}_{\text{f}}\right)\right]\right\} \quad (1)$$

$$\text{mean\_AVG}_l = \frac{1}{60}\left\{\sum_{\text{f}=1}^{60}\left[\frac{1}{4}\left(\sum_{\text{lbr}=1}^{4}\text{IL\_L}_{\text{lbr}}\text{\_l}_{\text{f}}\right)\right]\right\} \quad (2)$$

2.9. sEMG fatigue signal acquisition and feature analysis

Each sEMG sensor channel adopted a three-electrode differential configuration to maximize the suppression of common-mode interference. According to the Nyquist–Shannon sampling theorem [42, 43], to achieve aliasing-free sEMG signal collection, the sampling frequency of the sEMG sensor was set to 1000 Hz.

Electrode placement: a dual-electrode scheme was adopted on each side, with a pair of electrodes spaced ≥ 2 cm apart, placed longitudinally along the erector spinae muscle group, 2–4 cm lateral to the spinous processes of L1–L5, and the ground electrode was placed in the sacral region between S1 and S3 (Figure 1). Before the experiment, 95% alcohol was used to wipe the electrode attachment sites to remove oil and cutin from the skin surface. The wearing position of the sEMG sensor is shown in Figure 1.

Fatigue induction and perception: the subjects rested fully before task execution. During the test, the subjects tried their best to maintain the standard posture until they reported involuntary tremor or the researchers observed posture deviation, and then the sEMG recording was stopped. This method is widely used in the induction and evaluation of muscle fatigue [44–47].

Feature analysis:

Continuous wavelet transform (CWT): characterizes the time-frequency characteristics of sEMG signals in each sensor channel during the entire fatigue process. CWT can effectively capture dynamic changes related to muscle fatigue [15, 48, 49].

Frequency band energy distribution: characterizes the proportion of sEMG frequency band energy during fatigue. Studies have shown that this distribution can reflect different stages of muscle fatigue [15, 50].

Median frequency (MDF): characterizes the muscle fatigue characteristics during the test. A decrease in MDF is usually associated with increased muscle fatigue [15, 50].

Median frequency: characterizes the muscle fatigue properties during the test. A decrease in MDF is typically associated with increasing muscle fatigue [51, 52].

Root mean square (RMS): analyzes the changes in muscle activation/inactivation characteristics during task execution under different postures. Changes in RMS value reflect the degree of muscle activation [53, 54].

2.10. Data analysis

2.10.1. Data processing

The lumbar joint angles of the three postures were normalized by Max–Min according to their maximum flexion angle range.

The flexion joint torques under the two lateral bridge postures were normalized by Max–Min according to their maximum torque range.

The IL and LTpL force data under the left and right lateral bridge postures were normalized by Max–Min according to their respective maximum ranges.

The CWT results of sEMG signals and the energy intensity of time-frequency profiles of each channel were normalized by Max–Min.

Morlet wavelet was used as the basis function for CWT analysis, with 32 scales per octave and a total of 287 scales. The sEMG energy was divided into five frequency bands (0–20 Hz, 20–60 Hz, 60–90 Hz, 90–150 Hz, 150–500 Hz), and the muscle fatigue stage was quantified by the proportion of frequency band energy (detailed calculation parameters and formulas see Supporting Information S2.10.1-1).

During the entire fatigue-inducing process, the sEMG signal was evenly divided into three parts. After calculating the MDF value of each part, the least squares method was used to fit the slope (fitting equation: $y = p_1x + p_2$), and the fitting effect was verified by the sum of squared residuals (detailed residual calculation method see Supporting Information S2.10.1-2).

The RMS value was used to reflect the degree of muscle activation, and the calculation logic was the square root of the average of the squared signal collection values (detailed calculation formula see Supporting Information S2.10.1-3).

2.10.2. Statistical analysis

Frequency band energy: paired sample t-test (Wilcoxon signed-rank test was used due to possible non-normal distribution) was used to analyze the changes in the proportion of energy in specific frequency bands between activated and inactivated muscles and compare the average proportion differences in specific frequency bands (such as 20–60 Hz, 90–150 Hz, grouped by 10 Hz increments). The significance level was set to $\alpha = 0.05$ [55].

Median frequency: paired sample t-test (Wilcoxon signed-rank test) was used to estimate the MDF difference between the non-fatigue segment (first 1/3 of the signal) and the fatigue segment (last 1/3 of the signal) under each activity state (paired by the non-fatigue MDF and fatigue MDF of each active/inactive state). The significance level was set to $\alpha = 0.05$ [56].

Root mean square: paired sample t-test (Wilcoxon signed-rank test) was used to estimate the RMS difference between activated and inactivated muscles within each posture group (paired by the RMS of activated muscles and the RMS of inactivated muscles). The significance level was set to $\alpha = 0.05$ [34].

All data were expressed as mean ± standard error (SE), and graphs were presented as mean ± standard deviation (SD). The significance level was defined as $p < 0.05$.

3. Results

3.1. Lumbar joint angles and torques

Under static experimental postures, the change in joint angle was extremely small. The temporal change of angle was mainly attributed to muscle fatigue [57, 58], changes in muscle tension, and nervous system regulation during posture maintenance. Figure 5 shows that the fluctuation of lumbar joint angles in the three postures within the min–max normalized range was very small (see Supporting Information Figure S1 for the original angle data graph).

3.2. Estimation of joint torque

The torques on the intervertebral discs calculated by inverse dynamics under three postures are shown in Figure 6: (a) quiet standing, (b) left lateral bridge, and (c) left bird-dog posture. Each group shows the bending, flexion, and rotation forces of the lumbar intervertebral disc, respectively.

1) Under the left lateral bridge posture, the distribution patterns of the bending force (bending, denoted as IVD_{bendjnt}) and axial rotation force (rotation, denoted as IVD_{rotjnt}) of the L1–L5 intervertebral discs were consistent, both gradually increasing from L1–L2 to L4–L5, while the distribution of the flexion force (flexion, denoted as IVD_{jnt}) of the L2–L5 intervertebral discs was opposite to the above two forces, gradually decreasing from L2–L3 to L4–L5. The specific data are shown in Figure 7 and Table S1.
2) Under the left bird-dog posture, the distribution patterns of the bending force (bending, denoted as IVD_{bendjnt}) and axial rotation force (rotation, denoted as IVD_{rotjnt}) of the L1–L5 intervertebral discs were consistent, both gradually decreasing from L1–L2 to L4–L5, while the flexion force (flexion, denoted as IVD_{jnt}) of the L2–L3 to L4–L5 intervertebral discs gradually increased, as shown in Figure 8 and Table S2.

To intuitively show the torque distribution of the L1–L5 lumbar intervertebral discs under the left lateral bridge and left bird-dog postures, the torques borne by the bending, axial, and rotation forces of the lumbar intervertebral discs during the two posture tests were normalized. The average value of the four joint torques was the average within 300 frames, where "*f*" is the number of frames in 5 sec, "*type*" is the type of joint torque, "*joint*" is the number of the lumbar intervertebral disc, "L1–L2_$IVD_{\text{bendjnt_1}}$" (L1–L2 denotes the intervertebral joint between L1 and L2. For details, refer to the Lumbar Joint column in Supplementary Information Table S1.) is the joint bending torque of the L1–L2 lumbar intervertebral disc in the first frame of data (N·m), and *N* is the total number of frames, which was 300 frames in this experiment.

$$\text{TORQUE}_{type} = \frac{1}{300}\sum_{f=1}^{N} \text{Joint\_IVD}_{type\_f} \tag{3}$$

Figure 6
Intervertebral disc torques calculated by inverse dynamics under three postures: (a) quiet standing, (b) left lateral bridge, and (c) left bird-dog. Each group of diagrams shows the torques of bending, flexion, and axial rotation of the intervertebral disc (unit: N·m)

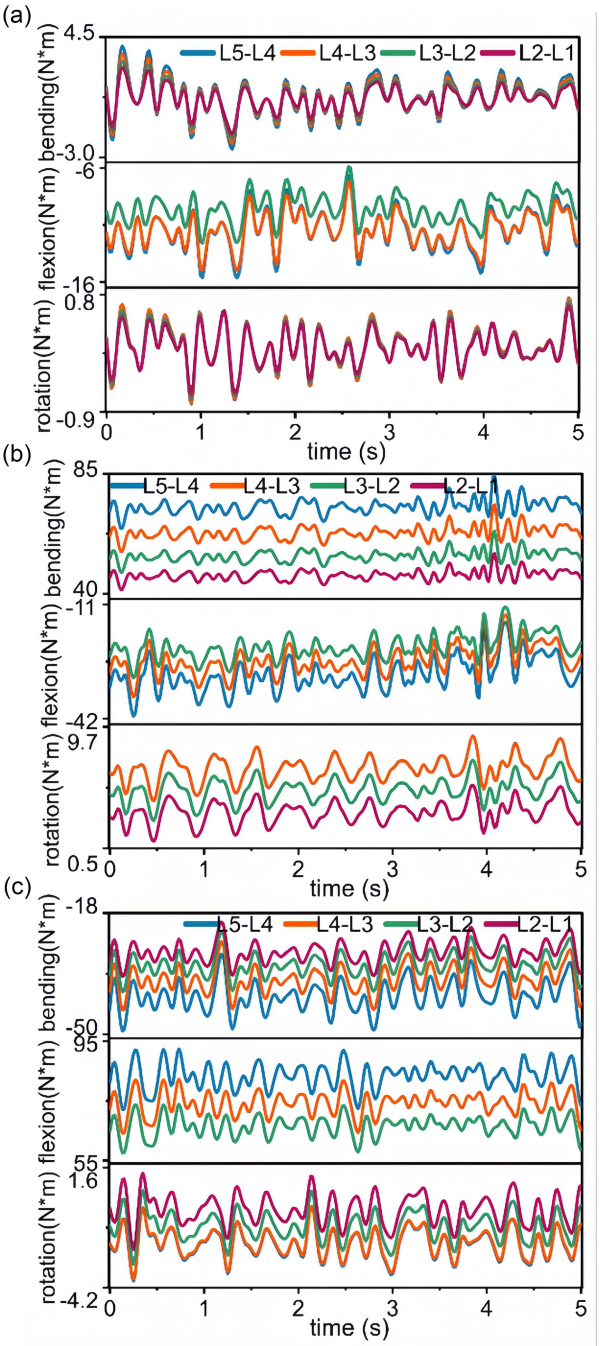

3.3. Lumbar joint muscle forces

The left lateral bridge posture was mainly maintained by the left muscles of the body, especially the erector spinae muscle group; similarly, the right lateral bridge posture was mainly maintained by the right erector spinae muscle group. The forces exerted by

Figure 7
(a) Torque distribution of bending, (b) flexion, and (c) rotation borne by L1–L5 lumbar intervertebral discs under left lateral bridge posture

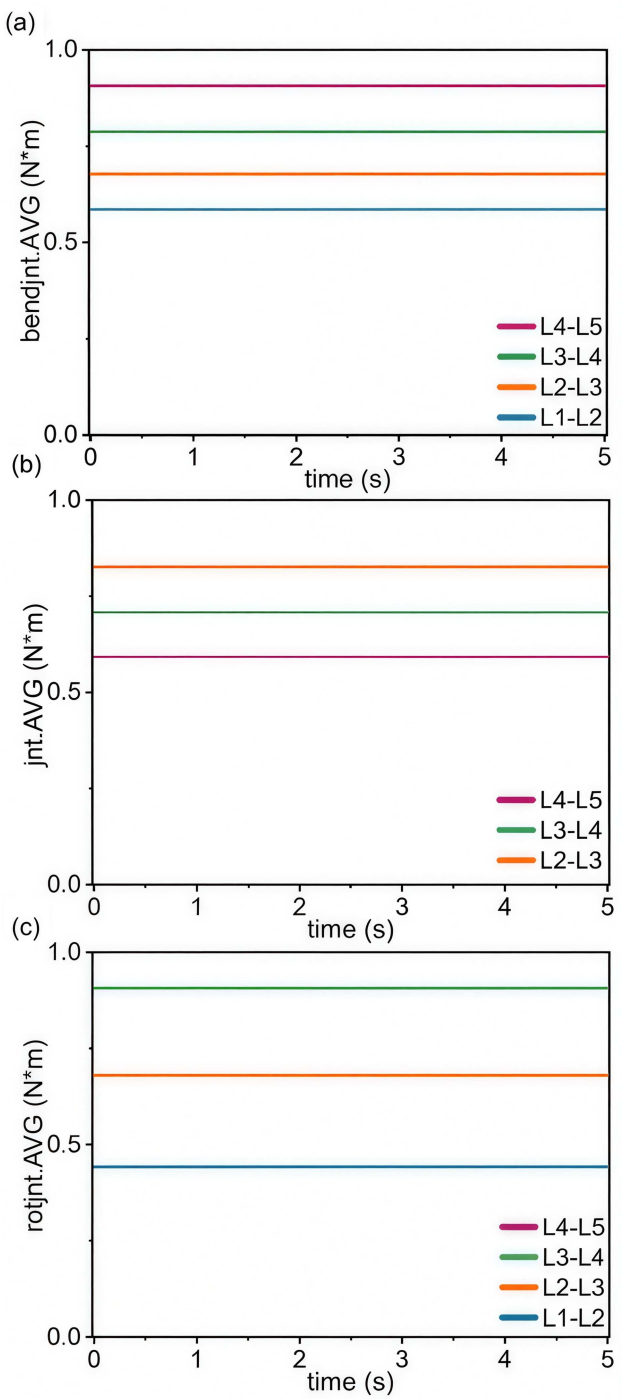

Figure 8
(a) Torque distribution of bending, (b) flexion, and (c) rotation borne by L1–L5 lumbar intervertebral discs under left bird-dog posture

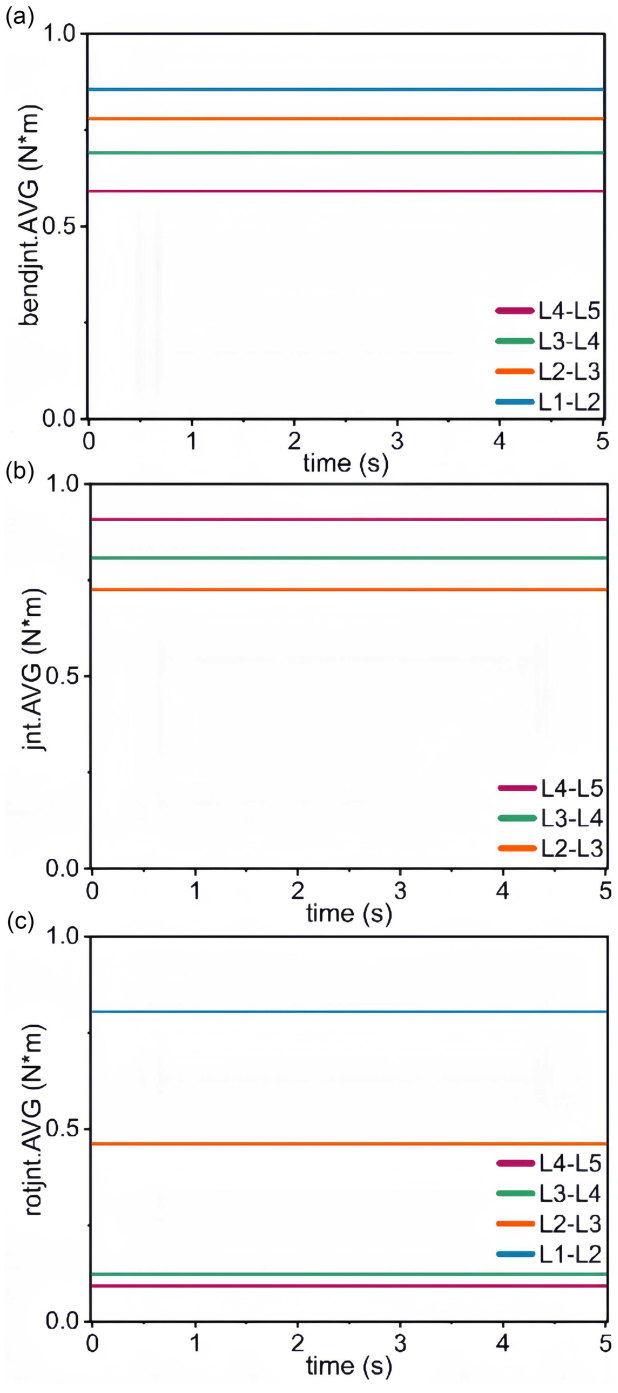

these related muscle groups on the lumbar joints are shown in Figures 9 and 10.

3.4. Lower back muscle fatigue analysis

To evaluate the degree of lumbar muscle fatigue under different postures, lateral bridge and bird-dog postures were used to induce fatigue, and the time–frequency domain characteristics of sEMG in the bilateral erector spinae region were characterized.

CWT was used to characterize the sEMG signal characteristics of each sensor channel during the entire muscle fatigue process. CWT can effectively capture dynamic changes related to muscle fatigue [48].

Figure 9
Forces exerted by the IL on L1–L4 lumbar joints: (a) the result of left lateral bridge posture and (b) the result of right lateral bridge posture

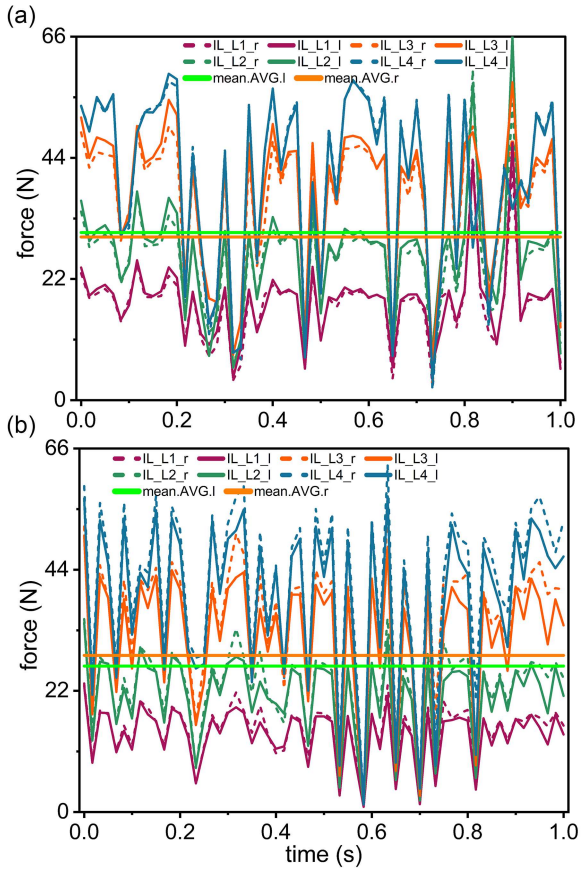

Figure 10
Forces exerted by the LTpL on L1–L5 lumbar joints: (a) the result of left lateral bridge posture and (b) the result of right lateral bridge posture

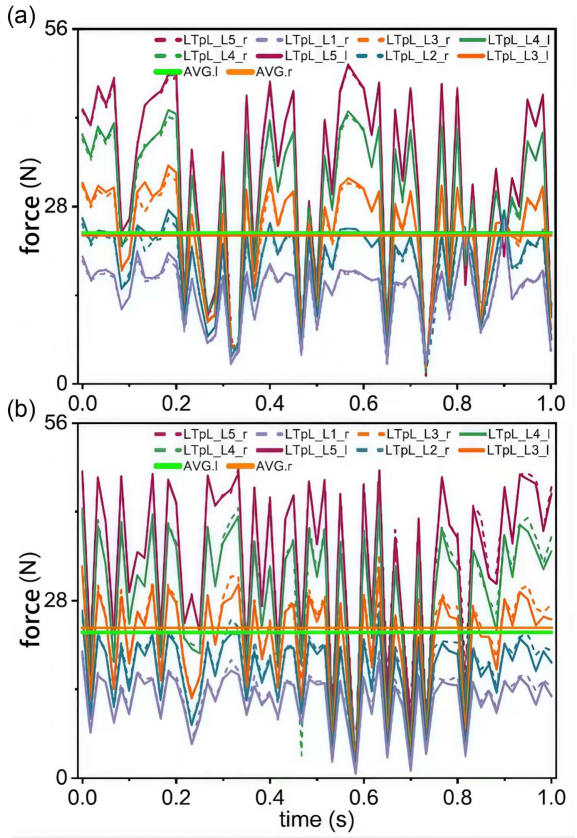

Figures 11 and 12 show the time-frequency energy evolution of sEMG signals under lateral bridge and bird-dog postures, respectively. The energy of activated muscles was mainly concentrated in the low-frequency band of 20–200 Hz, and there were differences in the time–frequency domain energy of bilateral channels under the same posture.

Band energy distribution charts characterize the temporal evolution of energy proportions across different sEMG frequency bands during fatigue. To analyze differences in frequency-domain energy distribution between muscle activation and non-activation states, sEMG frequencies were divided into five bands. The relative energy proportions of these bands are shown in Figure 13 (a, b, and c, d represent left- and right-side bridge dual-channel time-domain frequency band energy proportions) and Figure 14 (a, b, and c, d represent left and right bird-dog dual-channel time-domain frequency band energy proportions). Statistical analysis revealed regular patterns in the 20–60 Hz and 90–150 Hz frequency bands. Subsequently, paired *t*-tests (Wilcoxon signed-rank test) were employed to statistically evaluate the average differences between activated and non-activated states across groups. [55]

In the experiment, under specific postures and specific frequency bands, the difference between fatigue-induced muscles and non-induced muscles reached statistical significance. The results of the 20–60 Hz and 90–150 Hz frequency bands are shown in Figure 15 (all subjects).

Statistical results confirmed that there were significant differences in the energy proportion between activated and inactivated muscles in specific frequency bands (Figure 16):

Lateral bridge test: 87.5% of subjects (3/4) had extremely significant differences in the 20–60 Hz frequency band, and all subjects had significant differences in the 90–150 Hz frequency band.

Bird-dog test: 75% of subjects (3/4) had significant differences in the 20–60 Hz frequency band, and all subjects had extremely significant differences in the 90–150 Hz frequency band.

Paired sample *t*-test (Wilcoxon signed-rank test) was used for the four groups of tests to estimate the within-group differences (such as the average RMS of activated and inactivated muscles in each posture). The statistical analysis of RMS during fatigue induction is shown in Figure 17. Statistical results confirmed that there were significant differences between activated and inactivated states in specific frequency bands:

Lateral bridge test (Figure 16(a)): Left posture: there was a significant difference in the average RMS between activated and inactivated states ($p < 0.05$); right posture: there was no significant difference in the average RMS ($p > 0.05$)

Bird-dog test (Figure 16(b)): Left and right postures: there were significant differences in the average RMS between activated and inactivated states ($p < 0.05$) [34].

The sEMG signal of each fatigue induction test was divided into three segments (early stage = non-fatigue; middle stage; late stage = fatigue). Paired sample *t*-test (Wilcoxon signed-rank test) was used to compare the MDF between the non-fatigue segment (first 1/3) and the fatigue segment (last 1/3).

Figure 11
Time-frequency energy evolution of sEMG signals in two left and right lateral bridge tests: (a, b) channel 1 and (c, d) channel 2. Color represents normalized intensity

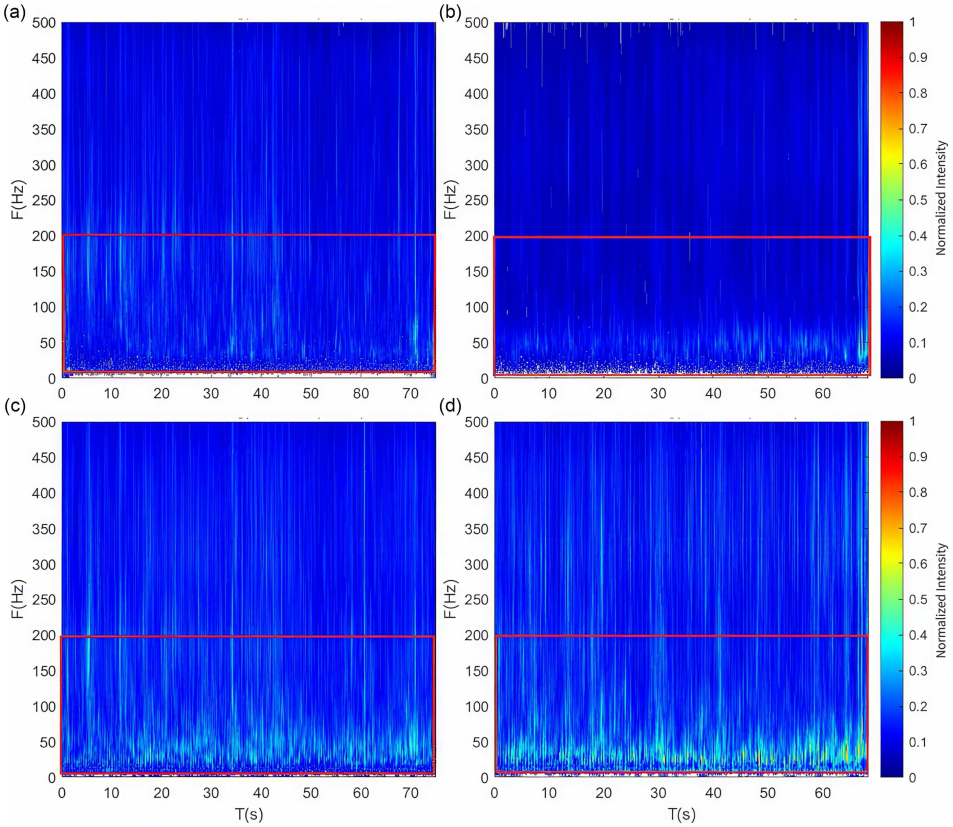

Figure 12
Time-frequency energy evolution of sEMG signals in two left and right bird-dog tests: (a, b) channel 1 and (c, d) channel 2. Color represents normalized intensity

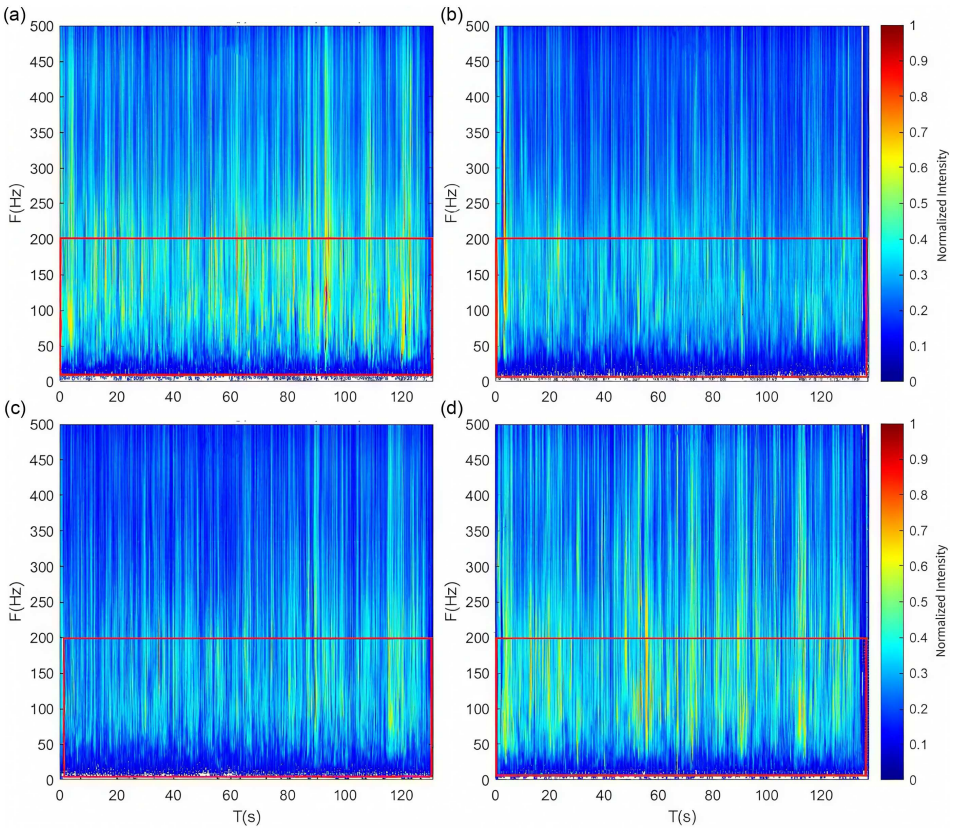

Figure 13

Changes in the proportion of sEMG signal band energy over time (*T*(s)) in two lateral bridge tests: (a, b) channel 1 and (c, d) channel 2. The color bar represents the relative energy contribution of different frequency bands: 0–20 Hz, 20–60 Hz, 60–90 Hz, 90–150 Hz, 150–500 Hz

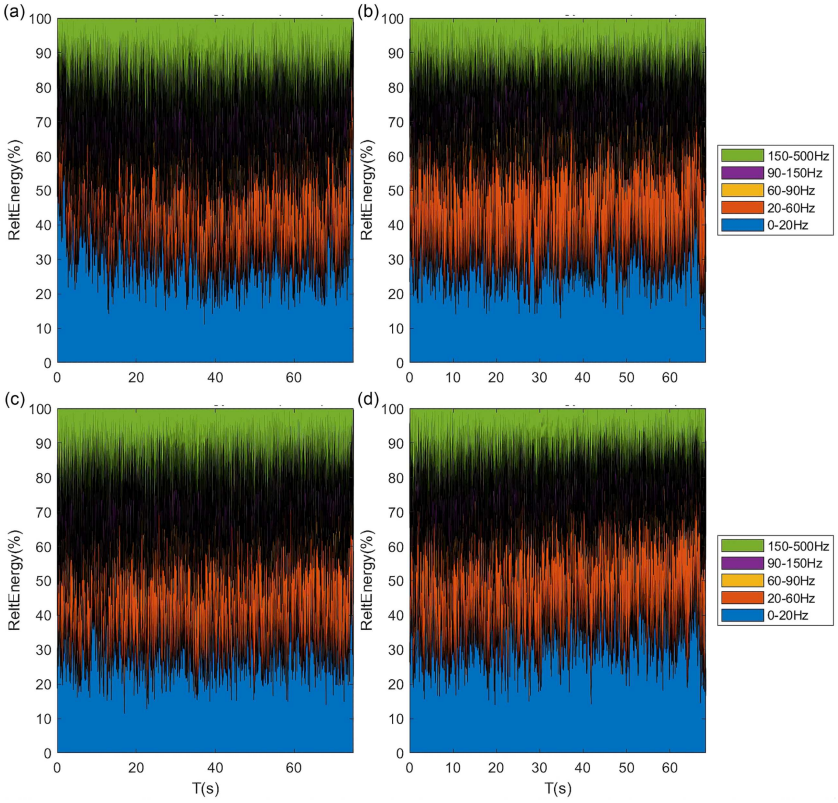

Figure 14

Percentage change in surface electromyographic signal energy across frequency bands over time during two bird-dog tests: (a, b) channel 1 and (c, d) channel 2. Color scale indicates relative energy contribution of different bands: 0–20 Hz, 20–60 Hz, 60–90 Hz, 90–150 Hz, 150–500 Hz

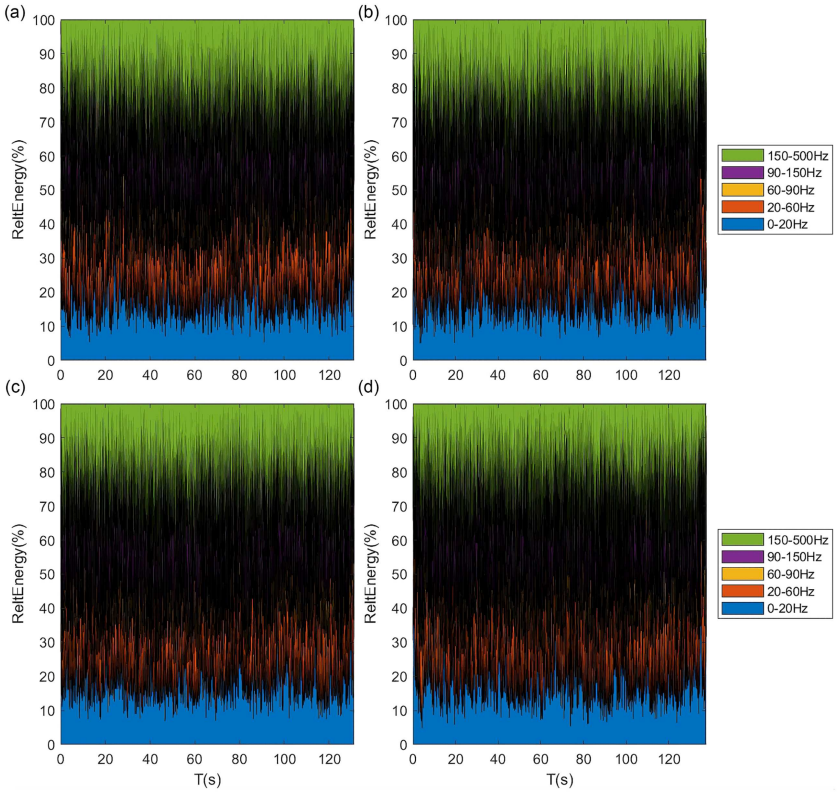

Note: The definition is consistent with Figure 13.

Figure 15

Differences in band energy proportion between activated muscles (sEMG channel 1) and inactivated muscles (sEMG channel 2) during fatigue induction: (a, b) 20–60 Hz and 90–150 Hz frequency bands under lateral bridge posture of four subjects; (c, d) 20–60 Hz and 90–150 Hz frequency bands under bird-dog posture of four subjects. ($^{*}p < 0.05$; $^{**}p < 0.01$, using paired Wilcoxon test)

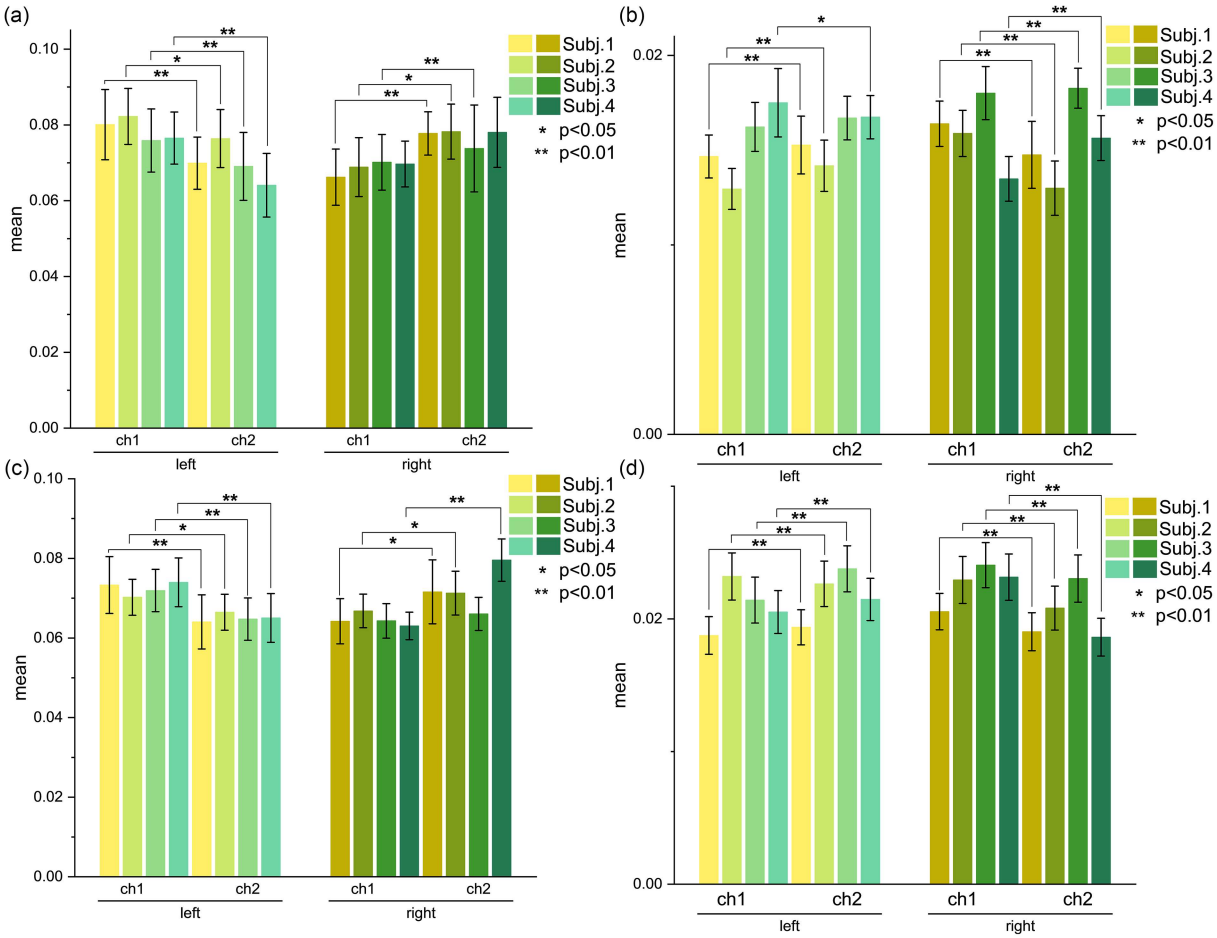

Note: Detailed data such as specific p-values and statistics for each subject are shown in the supplementary materials: detailed description in Figure 15.

Figure 16

Experimental average RMS values: (a) RMS values of left and right lateral bridge tests of four subjects, with the bar chart representing the average RMS values of activated and inactivated muscles, and (b) RMS values of left and right bird-dog tests of four subjects. ($^{*}p < 0.05$, indicating a significant difference between activated and inactivated muscles of the posture/subject)

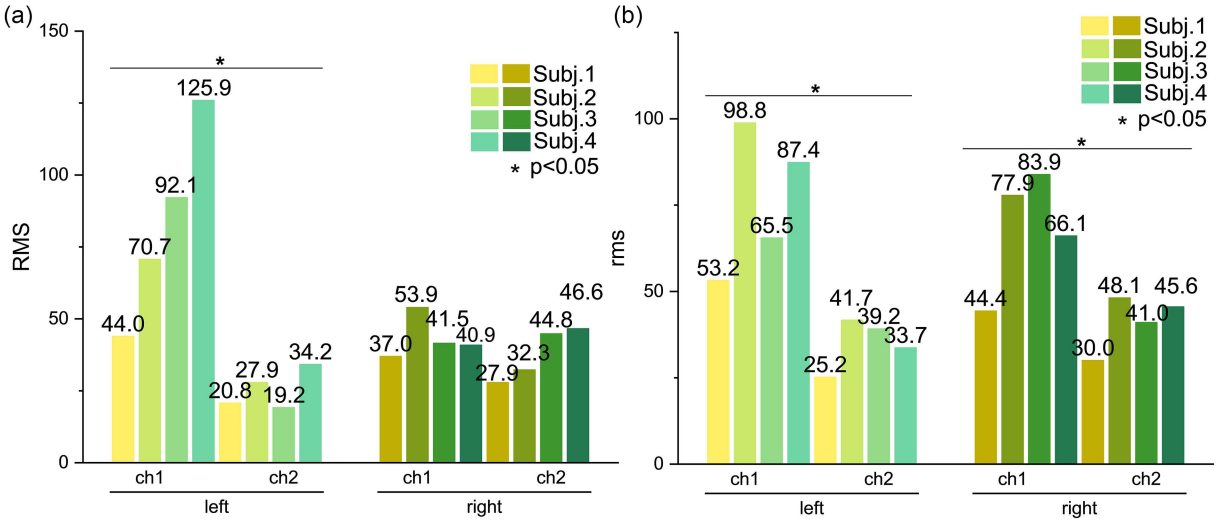

Figure 17

Changes in MDF before and after fatigue induction: (a) lateral bridge posture test and (b) bird-dog posture test. Data represent the MDF values (unit: Hz) of activated (channel 1) and inactivated (channel 2) sEMG channels before and after fatigue. (*$p < 0.05$)

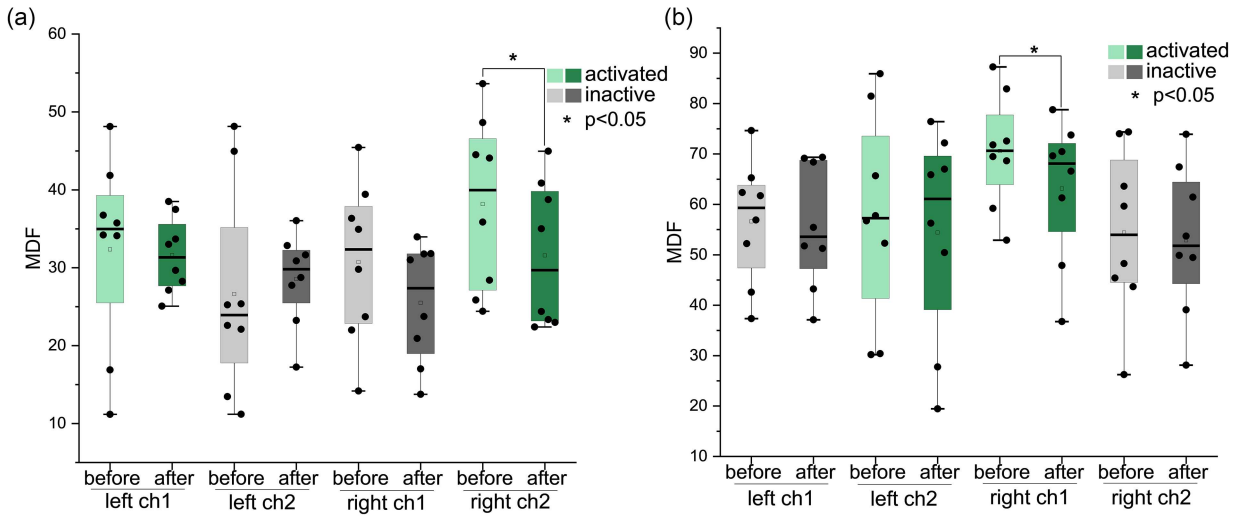

Statistical results showed:

Lateral bridge test (Figure 16(a)): Right posture: MDF after fatigue induction was significantly lower than that before fatigue ($p < 0.05$).

Bird-dog test (Figure 16(b)): Right posture: MDF after fatigue induction was significantly lower than that before fatigue ($p < 0.05$), and the median decreased with the occurrence of fatigue.

4. Discussion

This experiment verified the performance of IMU sensors in evaluating the 3D joint angle, torque, and local muscle force of the L1–L5 lumbar segments and tested four types of static postures (including six movements) (Figure 4). Initially, we hypothesized that the biological motion information captured by IMUs, after conversion, could serve as a reliable basis for biomechanical simulation solving in OpenSim [59]. The experimental results generally met this expectation, providing methodological support for the noninvasive assessment of static lumbar self-load in real environments.

The traditional common method for biomechanical analysis in OpenSim relies on marker trajectory files obtained by OMC systems, but OMC systems have limitations such as environmental constraints and high equipment costs. Opensense only supports a limited range of IMU sensor models. To adapt to the IMU sensors used in this experiment, we adopted the BVH file format exported by the sensors and successfully generated OpenSim-compatible marker trajectory files (.trc) through a self-developed two-stage Python script conversion process, realizing the docking of motion data in non-laboratory environments with musculoskeletal simulation models. The effectiveness of this data conversion scheme was supported by the experimental results: under static postures such as lateral bridge, quiet standing, and bird-dog, the maximum range of lumbar joint angle change during posture maintenance was only 0.018° (Figure 5). This slight fluctuation can be attributed to extremely slight "jitter" or noise, indicating that the motion data collected by IMUs can reliably reconstruct and retain the core biomechanical information of the human lumbar spine in real environments [60–62].

We further evaluated the distribution characteristics of intervertebral disc joint forces under different static postures: under the left lateral bridge posture, the bending and axial rotation forces gradually increased from L1–L2 to L4–L5, while the flexion force showed an opposite decreasing trend; under the left bird-dog posture, the opposite force distribution pattern was presented, with the maximum intersegmental torque difference reaching 25.68 N·m (between L4–L5 and L1–L2 under the left lateral bridge posture) (Figures 7 and 8; Tables S1 and S2). This finding suggests that different static working postures or daily body postures may lead to significant differences in the load of each lumbar segment, providing a mechanical basis for subsequent research on posture optimization and injury prevention for specific occupational groups (such as long-term sitting office workers). The static optimization results further confirmed the rationality of the simulation: in the lateral bridge posture, the forces exerted by the IL and LTpL on the lumbar joints on the posture-maintaining side were significantly greater than those on the contralateral side (Figures 9 and 10; Table S3), which was highly consistent with the physiological mechanism of muscle activation when the human body maintains static balance.

The time–frequency domain analysis of lumbar sEMG signals provided supplementary verification for the simulation results: during fatigue induction, the sEMG energy of activated muscles was mainly concentrated in the low-frequency band of 20–200 Hz, and there were statistically significant differences in the energy proportion of the 20–60 Hz and 90–150 Hz frequency bands between activated and inactivated muscles (Figure 15); the RMS value was significantly increased in activated muscles, and the MDF was significantly decreased with the progress of fatigue (Figures 16 and 17). These characteristics were consistent with the known physiological laws of muscle fatigue [51, 52], further confirming the reliability of the IMU-sEMG combined system in evaluating static lumbar load.

Compared with existing related studies, the core incremental contribution of this study lies in focusing on the assessment of static postures in real environments—a scenario ignored by existing studies (existing studies mostly focus on dynamic tasks or laboratory-controlled environments [16, 63]). Wenghofer et al. [64] constructed a markerless system using RGB-D cameras, which is

suitable for clinical dynamic spinal motion assessment but has limited applicability in the special analysis of static sitting postures in office scenarios; Zhang et al. [16] evaluated lumbar load during walking through the OMC system, and its dynamic force distribution pattern was significantly different from the static results of this study, while the OMC system cannot be applied to natural office environments; de Carvalho et al. [63] only evaluated the impact of office chair design on lumbar posture through sEMG, without involving the quantitative analysis of lumbar joint torque and muscle force. This study, through the integration of IMU and sEMG combined with OpenSim simulation, realized the integrated assessment of lumbar kinematics, dynamics, and muscle fatigue under static postures in natural environments for the first time, filling the research gap in this field.

This study has three key limitations that need to be clearly stated and provide directions for future research:

Limitation of sample size: only four healthy young male volunteers were included, which severely limited the statistical test power and the reliability of between-group variation analysis. Lumbar biomechanical characteristics may vary significantly due to gender (such as differences in muscle mass and pelvic structure), age (such as muscle strength decline and joint degeneration in the elderly), and health status (such as muscle compensatory activation in patients with low back pain). Therefore, the results of this study cannot be generalized to women, the elderly, or patients with low back pain and can only reflect the lumbar load characteristics of healthy young men under specific static postures.

Lack of quantitative validation reference: no quantitative comparative validation was conducted with the gold standard of motion capture (OMC system) or direct force measurement equipment. Although the stability of IMU data and the physiological consistency of simulation results were confirmed, the absolute error between the evaluation results of this system and the "true" lumbar load cannot be clarified. This limitation may affect the absolute accuracy of the results. Future research needs to supplement synchronous tests with the OMC system to quantify the consistency of the two methods, such as quantifying consistency through Bland-Altman analysis and calculating the intraclass correlation coefficient and other indicators to further verify the quantitative reliability of the system.

Limitation of posture representativeness: the four types of static postures used in the experiment (quiet standing, sitting, lateral bridge, bird-dog) are all standardized test postures. Although they can effectively induce muscle fatigue and capture lumbar load characteristics, it is difficult to fully replicate the diverse static postures in daily life and work (such as leaning forward while seated or working sideways), which may limit the practical applicability of the results across different scenarios.

Additionally, the inherent accuracy limitations of IMU sensors may result in insufficient statistical significance for muscle-driven joint forces. Future improvements could be achieved by optimizing sensor calibration processes, increasing data sampling frequency, or integrating multi-sensor data.

5. Conclusion

The comprehensive experimental results show that the OpenSim musculoskeletal simulation driven by biological data collected by IMUs can accurately assess the lumbar joint angle, torque, and related muscle group load of healthy young male volunteers under specific static postures at the methodological level, and its results are highly consistent with known biomechanical principles and muscle physiological characteristics. Inverse kinematics results show that the lumbar (L1–L5) joint angle has good stability under static conditions, the joint torque distribution presents a clear posture-dependent law, and the sEMG signal effectively captures the characteristics of muscle activation and fatigue progression, confirming the internal consistency and reliability of the evaluation system. Compared with the OMC system, the portability and environmental adaptability of IMU sensors make them more suitable for static lumbar load monitoring in real work scenarios, providing a new technical path for noninvasive evaluation in related fields.

Limited by the sample size, lack of gold-standard quantitative verification, and insufficient posture representativeness, the results of this study are only a verification of methodological effectiveness, not an inference at the population level or direct clinical application. Future research should prioritize three tasks: (1) expand the sample size and include a diverse population (including different genders, ages, and health statuses) to improve the generalizability of the results; (2) conduct synchronous comparison with the OMC system and direct force measurement equipment to quantitatively evaluate the absolute accuracy and consistency of the evaluation system; and (3) expand the types of test postures, include more typical static postures in daily life and work, and enhance the practical application value of the results. On this basis, the feasibility of developing a nonspecific low back pain risk screening tool based on the IMU-sEMG combined sensor system can be further explored, providing technical support for the early intervention and occupational health protection of this disease.

Acknowledgment

The authors would like to express their gratitude to the Guangdong Academy of Sciences and ZhuJiang Hospital of Southern Medical University for their support in this work. Special thanks are also extended to Prof. Guozhi Huang and Dr. Qing Zeng for their contributions.

Funding Support

This work is supported by the GDAS' Project of Science and Technology Development (2024GDASZH-2024010101).

Ethical Statement

The study was conducted in accordance with the principles outlined in the Declaration of Helsinki and approved by the Medical Ethics Committee of ZhuJiang Hospital of Southern Medical University (Protocol code: 2023-KY-008-02).

Conflicts of Interest

The authors declare that they have no conflicts of interest to this work.

Data Availability Statement

Data are available from the corresponding author upon reasonable request.

Author Contribution Statement

Zhong Wang: Methodology, Software, Validation, Formal analysis, Investigation, Data curation, Writing – original

draft, Visualization. **Xiaohuan Yuan:** Writing – review & editing, Supervision. **Yuanliang Tang:** Conceptualization, Resources, Writing – review & editing, Supervision. **Shaohui Zhang:** Conceptualization, Resources, Writing – review & editing, Supervision, Project administration, Funding acquisition.

References

[1] Bavi, O., Ozmaeian, M., & Heydari, M. H. (2022). Biomechanics and mechanobiology. *Frontiers in Mechanical Engineering*, *8*, 863175. https://doi.org/10.3389/fmech.2022.863175

[2] Seth, A., Hicks, J. L., Uchida, T. K., Habib, A., Dembia, C. L., Dunne, J. J., . . . , & Delp, S. L. (2018). OpenSim: Simulating musculoskeletal dynamics and neuromuscular control to study human and animal movement. *PLoS Computational Biology*, *14*(7), e1006223. https://doi.org/10.1371/journal.pcbi.1006223

[3] Evans, M., Needham, L., Wade, L., Parsons, M., Colyer, S., McGuigan, P., . . . , & Cosker, D. (2024). Synchronised video, motion capture and force plate dataset for validating markerless human movement analysis. *Scientific Data*, *11*(1), 1300. https://doi.org/10.1038/s41597-024-04077-3

[4] Yang, J. (2024). Analysis of motion capture technology research and typical applications. *Applied and Computational Engineering*, *112*(1), 130–138. https://doi.org/10.54254/2755-2721/2024.17920

[5] Yu, Z., Zahid, A., Ansari, S., Abbas, H., Heidari, H., Imran, M. A., & Abbasi, Q. H. (2022). IMU sensing–based Hopfield neuromorphic computing for human activity recognition. *Frontiers in Communications and Networks*, *2*, 820248. https://doi.org/10.3389/frcmn.2021.820248

[6] Cox, J., Zhang, W., & Furukawa, T. (2023). Motion tracking with coupled magnetometers and dynamic IMU measurement fusion in nonuniform magnetic fields. In *2023 26th International Conference on Information Fusion*, 1–8. https://doi.org/10.23919/FUSION52260.2023.10224146

[7] Sun, Y., Song, Z., Mo, L., Li, B., Liang, F., Yin, M., & Wang, D. (2025). IMU-based quantitative assessment of stroke from gait. *Scientific Reports*, *15*(1), 9541. https://doi.org/10.1038/s41598-025-94167-y

[8] Favata, A., Gallart-Agut, R., Pàmies-Vilà, R., Torras, C., & Font-Llagunes, J. M. (2024). IMU-based systems for upper limb kinematic analysis in clinical applications: A systematic review. *IEEE Sensors Journal*, *24*(18), 28576–28594. https://doi.org/10.1109/JSEN.2024.3436532

[9] Tarmizi, M. I., Hamid, A., & Yusof, Y. (2025). Smart Shoe: Portable gait monitoring system utilizing inertial measurement unit (IMU). *Jurnal Mekanikal*, *48*(1), 107–118. https://doi.org/10.11113/jm.v48.561

[10] Kárason, H., Ritrovato, P., Maffulli, N., Boccaccini, A. R., & Tortorella, F. (2024). Wearable approaches for non-invasive monitoring of tendons: A scoping review. *Internet of Things*, *26*, 101199. https://doi.org/10.1016/j.iot.2024.101199

[11] Wang, S., Tang, H., Wang, B., & Mo, J. (2021). Analysis of fatigue in the biceps brachii by using rapid refined composite multiscale sample entropy. *Biomedical Signal Processing and Control*, *67*, 102510. https://doi.org/10.1016/j.bspc.2021.102510

[12] Suganthi, J. R., & Rajeswari, K. (2023). Evaluation of muscle fatigue based on sEMG using deep learning techniques. In *2023 5th International Conference on Inventive Research in Computing Applications*, 01–06. https://doi.org/10.1109/ICIRCA57980.2023.10220926

[13] Li, N., Zhou, R., Krishna, B., Pradhan, A., Lee, H., He, J., & Jiang, N. (2024). Non-invasive techniques for muscle fatigue monitoring: A comprehensive survey. *ACM Computing Surveys*, *56*(9), 1–40. https://doi.org/10.1145/3648679

[14] Wang, S., Tang, H., Wang, B., & Mo, J. (2023). A novel approach to detecting muscle fatigue based on sEMG by using neural architecture search framework. *IEEE Transactions on Neural Networks and Learning Systems*, *34*(8), 4932–4943. https://doi.org/10.1109/TNNLS.2021.3124330

[15] Shariatzadeh, M., Hafshejani, E. H., Mitchell, C. J., Chiao, M., & Grecov, D. (2023). Predicting muscle fatigue during dynamic contractions using wavelet analysis of surface electromyography signal. *Biocybernetics and Biomedical Engineering*, *43*(2), 428–441. https://doi.org/10.1016/j.bbe.2023.04.002

[16] Zhang, Z., Zou, J., Lu, P., Hu, J., Cai, Y., Xiao, C., . . . , & Huang, G. (2024). Analysis of lumbar spine loading during walking in patients with chronic low back pain and healthy controls: An OpenSim-based study. *Frontiers in Bioengineering and Biotechnology*, *12*, 1377767. https://doi.org/10.3389/fbioe.2024.1377767

[17] Urukalo, D., Nates, F. M., & Blazevic, P. (2024). Sensor placement determination for a wearable device in dual-arm manipulation tasks. *Engineering Applications of Artificial Intelligence*, *137*, 109217. https://doi.org/10.1016/j.engappai.2024.109217

[18] Fujii, R., Takahashi, Y., Tsuichihara, S., & Yamada, T. (2025). Assist control of lifting motion of lumbar-powered exoskeleton using IMU sensors. *Journal of Advanced Computational Intelligence and Intelligent Informatics*, *29*(3), 559–573. https://doi.org/10.20965/jaciii.2025.p0559

[19] Stienen, M. N., Ho, A. L., Staartjes, V. E., Maldaner, N., Veeravagu, A., Desai, A., . . . , & Park, J. (2019). Objective measures of functional impairment for degenerative diseases of the lumbar spine: A systematic review of the literature. *The Spine Journal*, *19*(7), 1276–1293. https://doi.org/10.1016/j.spinee.2019.02.014

[20] Fang, G., Lin, Y., Wu, J., Cui, W., Zhang, S., Guo, L., . . . , & Huang, W. (2020). Biomechanical comparison of standalone and bilateral pedicle screw fixation for oblique lumbar interbody fusion surgery—A finite element analysis. *World Neurosurgery*, *141*, e204–e212. https://doi.org/10.1016/j.wneu.2020.05.245

[21] Bontrup, C., Taylor, W. R., Fliesser, M., Visscher, R., Green, T., Wippert, P.-M., & Zemp, R. (2019). Low back pain and its relationship with sitting behaviour among sedentary office workers. *Applied Ergonomics*, *81*, 102894. https://doi.org/10.1016/j.apergo.2019.102894

[22] Sulaiman, H. M., & Zafar, S. (2023). A review on effects of exercises therapy for office workers with chronic no specific low back pain. *Clinical Medicine and Health Research Journal*, *3*(6), 663–670. https://doi.org/10.18535/cmhrj.v3i6.284

[23] Lu, M.-L. (2020). Prevention of musculoskeletal pain among professional drivers. *Journal of Occupational Health*, *62*(1), e12170. https://doi.org/10.1002/1348-9585.12170

[24] Swathi, S., Senthil, P., & Neelam, S. (2022). Nonspecific low back pain in sedentary workers: A narrative review. *Biomedicine*, *42*(5), 863–869. https://doi.org/10.51248/.v42i5.1484

[25] Saiklang, P., Chatprem, T., Karoonsupcharoen, O., Saiklang, P., & Puntumetakul, R. (2024). The comparison of the effect of prolonged sitting on lumbar repositioning error in asymptomatic and chronic low back pain participants with seated

sedentary behavior. *Trends in Sciences*, *21*(3), 7332. https://doi.org/10.48048/tis.2024.7332

[26] Amiri, B., Behm, D. G., & Zemková, E. (2025). On the role of core exercises in alleviating muscular fatigue induced by prolonged sitting: A scoping review. *Sports Medicine—Open*, *11*(1), 18. https://doi.org/10.1186/s40798-025-00816-x

[27] Wirth, B., & Schweinhardt, P. (2024). Personalized assessment and management of non-specific low back pain. *European Journal of Pain*, *28*(2), 181–198. https://doi.org/10.1002/ejp.2190

[28] Shim, G. Y., Choi, J., Kim, H. J., Kwon, R., Kim, M. S., Yoo, M. C., . . . , & Yon, D. K. (2024). Global, regional, and national burden of spine pain, 1990-2019: A systematic analysis of the global burden of disease study 2019. *Archives of Physical Medicine and Rehabilitation*, *105*(3), 461–469. https://doi.org/10.1016/j.apmr.2023.10.019

[29] Du, M., Lv, B., Fan, B., Li, X., Yu, J., Yi, F., . . . , & Cai, S. (2024). Ankle moment estimation based on a novel distributed plantar pressure sensing system. *IEEE Journal of Biomedical and Health Informatics*, *28*(11), 6548–6556. https://doi.org/10.1109/JBHI.2024.3444818

[30] Vanhauter, N., van Erck, A., Anciaux, M., Pollefliet, A., & Joos, E. (2021). Isometric and isokinetic muscle strength measurements of the lumbar flexors and extensors with BioniX Sim3 Pro in patients with chronic low back pain: A pilot study. *Journal of Back and Musculoskeletal Rehabilitation*, *34*(3), 381–388. https://doi.org/10.3233/BMR-200225

[31] Zhang, Y., Chen, M., Liu, H., He, Y., Li, Y., Shen, P., . . . , & Liu, C. (2024). Effect of different isometric trunk extension intensities on the muscle stiffness of the lumbar and lower limbs. *Frontiers in Physiology*, *14*, 1337170. https://doi.org/10.3389/fphys.2023.1337170

[32] Huang, T., & Kim, S. (2022). Immediate effect of trunk flexion and extension isometric exercise using an external compression device on electromyography of the hip extensor and trunk range of motion of healthy subjects. *BMC Sports Science, Medicine and Rehabilitation*, *14*(1), 116. https://doi.org/10.1186/s13102-022-00506-1

[33] Escamilla, R. F., Lewis, C., Pecson, A., Imamura, R., & Andrews, J. R. (2016). Muscle activation among supine, prone, and side position exercises with and without a Swiss ball. *Sports Health*, *8*(4), 372–379. https://doi.org/10.1177/1941738116653931

[34] Choi, C.-W., Koo, J.-W., & Jeong, Y.-G. (2023). An electromyographical comparison of torso muscle activity and ratio during modified side bridge exercises. *Journal of Back and Musculoskeletal Rehabilitation*, *36*(6), 1355–1363. https://doi.org/10.3233/BMR-220380

[35] Baijot, M., Puers, R., & Kraft, M. (2021). Monitoring lower back activity in daily life using small unintrusive sensors and wearable electronics in the context of rheumatic and musculoskeletal diseases. *Sensors*, *21*(19), 6362. https://doi.org/10.3390/s21196362

[36] Makrygiannis, D., Glushkova, A., Manitsaris, S., & Senteri, G. (2025). PosePilot—A web-based application for human motion data analysis and visualization. In *2025 IEEE 19th International Conference on Automatic Face and Gesture Recognition*, 1. https://doi.org/10.1109/FG61629.2025.11099475

[37] Fei, F., Yang, R., Li, J., Cao, Q., Zhang, Q., & Wu, C. (2024). Development of human motion capture system based on multiple inertial sensor units. In *2024 IEEE 14th International Conference on CYBER Technology in Automation, Control, and Intelligent Systems*, 173–178. https://doi.org/10.1109/CYBER63482.2024.10749165

[38] Armin, A. P., & Mandita, F. (2018). Variasi animasi gerakan menggunakan edit data BVH. *Fountain of Informatics Journal*, *3*(1), 1–4. https://doi.org/10.21111/fij.v3i1.1349

[39] Yoon, S., & Koo, S. (2025). A comparative study of ANN-based forward dynamics and inverse dynamics in human gait analysis. *Journal of Biomechanics*, *189*, 112800. https://doi.org/10.1016/j.jbiomech.2025.112800

[40] Pizzolato, C., Reggiani, M., Modenese, L., & Lloyd, D. G. (2017). Real-time inverse kinematics and inverse dynamics for lower limb applications using OpenSim. *Computer Methods in Biomechanics and Biomedical Engineering*, *20*(4), 436–445. https://doi.org/10.1080/10255842.2016.1240789

[41] Meszaros-Beller, L., Hammer, M., Schmitt, S., & Pivonka, P. (2023). Effect of neglecting passive spinal structures: A quantitative investigation using the forward-dynamics and inverse-dynamics musculoskeletal approach. *Frontiers in Physiology*, *14*, 1135531. https://doi.org/10.3389/fphys.2023.1135531

[42] Por, E., van Kooten, M., & Sarkovic, V. (2019). *Nyquist–Shannon sampling theorem*. *[Lecture Notes]. Department of Astronomy, Leiden University*. https://home.strw.leidenuniv.nl/~por/AOT2019/docs/AOT_2019_Ex13_NyquistTheorem.pdf

[43] Sarker, P., & Mirka, G. (2019). Effects of sampling frequency and sample window size on median frequency of surface EMG. *Proceedings of the Human Factors and Ergonomics Society Annual Meeting*, *63*(1), 1369–1372. https://doi.org/10.1177/1071181319631166

[44] Tabasi, A., Brouwer, N. P., Kingma, I., van Dijk, W., de Looze, M. P., Moya-Esteban, A., . . . , & van Dieën, J. H. (2023). The effect of back muscle fatigue on EMG and kinematics based estimation of low-back loads and active moments during manual lifting tasks. *Journal of Electromyography and Kinesiology*, *73*, 102815. https://doi.org/10.1016/j.jelekin.2023.102815

[45] Timbert, T., Amiez, N., Martin, A., Cometti, C., & Paizis, C. (2025). Effect of superimposed local vibration on neuromuscular fatigue during high-intensity intermittent isometric contractions in healthy adults. *Journal of Applied Physiology*, *139*(5), 1322–1333. https://doi.org/10.1152/japplphysiol.00582.2025

[46] Song, J., Choi, Y.-S., Lee, S., Park, D., & Park, J. (2025). Changes in muscle oxygenation and activity during cumulative isometric muscle contraction: New insight into muscle fatigue. *Frontiers in Physiology*, *16*, 1559893. https://doi.org/10.3389/fphys.2025.1559893

[47] Akagi, R., Hinks, A., & Power, G. A. (2020). Differential changes in muscle architecture and neuromuscular fatigability induced by isometric resistance training at short and long muscle-tendon unit lengths. *Journal of Applied Physiology*, *129*(1), 173–184. https://doi.org/10.1152/japplphysiol.00280.2020

[48] Di Nardo, F., Basili, T., Meletani, S., & Scaradozzi, D. (2022). Wavelet-based assessment of the muscle-activation frequency range by EMG analysis. *IEEE Access*, *10*, 9793–9805. https://doi.org/10.1109/ACCESS.2022.3141162

[49] Daniel, N., Malachowski, J., Sybilski, K., & Siemiaszko, D. (2024). Quantitative assessment of muscle fatigue during rowing ergometer exercise using wavelet analysis of surface

electromyography (sEMG). *Frontiers in Bioengineering and Biotechnology*, *12*, 1344239. https://doi.org/10.3389/fbioe.2024.1344239

[50] Nair, R. R., Venugopal, G., & Swaminathan, R. (2024). Analysis of muscle fiber type proportions in surface electromyography signals of athletes using reassigned Morlet scalogram. *IEEE Transactions on Instrumentation and Measurement*, *73*, 1–10. https://doi.org/10.1109/TIM.2024.3376019

[51] Ming, D., Wang, X., Xu, R., Qiu, S., Zhao, X., Qi, H., . . . , & Wan, B. (2014). sEMG feature analysis on forearm muscle fatigue during isometric contractions. *Transactions of Tianjin University*, *20*(2), 139–143. https://doi.org/10.1007/s12209-014-2181-2

[52] Hsu, L.-I., Lim, K.-W., Lai, Y.-H., Lin, Y.-L., Chen, Y.-J., Chen, C.-S., & Chou, L.-W. (2025). Turns-amplitude and power spectral analyses of surface EMG for assessing muscle fatigue and recovery during dynamic hand gripping. *Computers in Biology and Medicine*, *193*, 110430. https://doi.org/10.1016/j.compbiomed.2025.110430

[53] Gagnat, Y., Brændvik, S. M., & Roeleveld, K. (2020). Surface electromyography normalization affects the interpretation of muscle activity and coactivation in children with cerebral palsy during walking. *Frontiers in Neurology*, *11*, 202. https://doi.org/10.3389/fneur.2020.00202

[54] Li, W., Li, Z., Qie, S., Yang, H., Chen, X., Liu, Y., . . . , & Zhang, K. (2020). Analysis of the activation modalities of the lower limb muscles during walking. *Technology and Health Care*, *28*(5), 521–532. https://doi.org/10.3233/THC-191939

[55] Michelotti, A., Rongo, R., Valentino, R., D'Antò, V., Bucci, R., Danzi, G., & Cioffi, I. (2019). Evaluation of masticatory muscle activity in patients with unilateral posterior crossbite before and after rapid maxillary expansion. *European Journal of Orthodontics*, *41*(1), 46–53. https://doi.org/10.1093/ejo/cjy019

[56] Schwensow, D., Hohmuth, R., Malberg, H., & Schmidt, M. (2022). Investigation of muscle fatigue during on-water rowing using surface EMG. In *2022 44th Annual International Conference of the IEEE Engineering in Medicine & Biology Society*, 3623–3627. https://doi.org/10.1109/EMBC48229.2022.9872010

[57] Yang, C., Leitkam, S., & Côté, J. N. (2019). Effects of different fatigue locations on upper body kinematics and inter-joint coordination in a repetitive pointing task. *PloS One*, *14*(12), e0227247. https://doi.org/10.1371/journal.pone.0227247

[58] Babski-Reeves, K., & Calhoun, A. (2016). Muscle activity and posture differences in the sit and stand phases of sit-to-stand workstation use: A comparison of computer configurations. *IIE Transactions on Occupational Ergonomics and Human Factors*, *4*(4), 236–246. https://doi.org/10.1080/21577323.2016.1226991

[59] Horenstein, R. E., Lewis, C. L., Yan, S., Halverstadt, A., & Shefelbine, S. J. (2019). Validation of magneto-inertial measuring units for measuring hip joint angles. *Journal of Biomechanics*, *91*, 170–174. https://doi.org/10.1016/j.jbiomech.2019.05.029

[60] Morrow, M. M. B., Lowndes, B., Fortune, E., Kaufman, K. R., & Hallbeck, M. S. (2017). Validation of inertial measurement units for upper body kinematics. *Journal of Applied Biomechanics*, *33*(3), 227–232. https://doi.org/10.1123/jab.2016-0120

[61] Bonakdar, A., Riahi, N., Shakourisalim, M., Miller, L., Tavakoli, M., Rouhani, H., & Golabchi, A. (2025). Validation of markerless vision-based motion capture for ergonomics risk assessment. *International Journal of Industrial Ergonomics*, *107*, 103734. https://doi.org/10.1016/j.ergon.2025.103734

[62] Lee, W., Lin, J.-H., Bao, S., & Lin, K.-Y. (2019). Reliability and validity of a posture matching method using inertial measurement unit-based motion tracking system for construction jobs. In *ASCE International Conference on Computing in Civil Engineering 2019*, 589–597. https://ascelibrary.org/doi/abs/10.1061/9780784482438.074

[63] de Carvalho, D. E., & Callaghan, J. P. (2023). Effect of office chair design features on lumbar spine posture, muscle activity and perceived pain during prolonged sitting. *Ergonomics*, *66*(10), 1465–1476. https://doi.org/10.1080/00140139.2022.2152113

[64] Wenghofer, J., Beange, K. H. E., Ramos, W. C., Mavor, M. P., & Graham, R. B. (2024). Dynamic assessment of spine movement patterns using an RGB-D camera and deep learning. *Journal of Biomechanics*, *166*, 112012. https://doi.org/10.1016/j.jbiomech.2024.112012

How to Cite: Wang, Z., Yuan, X., Tang, Y., & Zhang, S. (2026). Verification of the Self-Load Assessment Capability of Inertial Measurement Units via Lumbar Musculoskeletal Simulation. *Smart Wearable Technology*. https://doi.org/10.47852/bonviewSWT62028348